Comparing Series Elasticity and Admittance Control for Haptic Rendering

Takamasa Horibe[1,2], Emma Treadway[2(✉)], and R. Brent Gillespie[2]

[1] Aerospace Engineering, Nagoya University, Furo-cho, Chikusa-ku, Nagoya, Japan
horibe.takamasa@j.mbox.nagoya-u.ac.jp
[2] Mechanical Engineering, University of Michigan, Ann Arbor, MI, USA
{etreadwa,brentg}@umich.edu

Abstract. While feedback control can be used to cause a motorized device to render the dynamic behavior of a virtual environment, this capacity inevitably breaks down at high frequencies where the rendered impedance reverts to the impedance of the device hardware. This situation amounts to a disadvantage for admittance display, for which hardware impedance is high. Series elastic actuators offer an attractive alternative with lower impedance at high frequencies, though stability considerations impose limits on the stiffest virtual environment that may be rendered. In this paper we explore the tradeoffs between admittance control and series elastic actuation with the use of analytical comparisons in the frequency domain backed up by experiments and complemented with a passivity analysis that accounts for an excess of passivity contributed by human biomechanics.

Keywords: Series elastic actuator · Admittance display · Passivity

1 Introduction

The design of a haptic device and its controllers is invariably a study in tradeoffs. In theory, rendering a programmable immitance[1] simply requires sourcing force in a certain relationship to sensed motion or sourcing motion in the inverse of that same relationship to sensed force. But pure force and motion sources cannot be found on the shelf and cannot even be built in a lab. Above a certain frequency, the mass used to build the device will necessarily foil any efforts to source force or motion, and the inherent dynamics of the device will dominate the immitance rendered at high frequencies.

Haptic display devices fall into two basic families: impedance display devices that function as force sources (sensing motion) and admittance display devices that function as motion sources (sensing force). An impedance display device usually employs motors with low rotor inertia in direct drive so that free space

[1] *Immitance* is a term that can be used to refer to the relationship between force and motion without specifying input and output, whereas admittance implies motion response to force and impedance implies force response to motion.

F. Bello et al. (Eds.): EuroHaptics 2016, Part I, LNCS 9774, pp. 240–250, 2016.
DOI: 10.1007/978-3-319-42321-0_22

may be rendered without feedback compensation—freespace impedance generally defaults to the inherent device impedance. As a consequence of using lower inertia motors in direct drive, however, force capacity is limited, and rendering a virtual wall is often hampered by force saturation. An admittance display device, on the other hand, uses powerful motors often outfitted with transmissions to render crisp and stiff virtual walls, but as a result, free space motion is in fact not very free. At high frequencies the rendered impedance reverts to the inherent device impedance, which is relatively high.

In this paper we explore the promise of series elasticity as an intermediate option between an impedance and an admittance device. We aim for a device design capable of rendering much free-er free space than a typical admittance device yet capable of sourcing higher forces than a typical impedance device.

A series elastic actuator (SEA) features a physical spring introduced between a geared motor and the load [8]. A SEA can be considered a special class of variable impedance actuator (VIA), but with a fixed compliance. VIAs use software control and hardware to render varying impedances [14]. SEAs have found wide acceptance in applications such as legged robotics, where tolerance to shock loading is of paramount concern. Other significant advantages to SEA have been pointed out in the literature, including filtering and masking of motor- and gear-induced nonlinearities to produce a clean force output, masking of high inertia, low inherent impedance, and conversion of a force-control problem into a position-control one [9,10,13]. Series elastic actuators inherently feature energy-storage as well [8].

A number of papers treating series elasticity have suggested its application to haptic interfaces because of the clean force output [9,10]. Our group explored free-space rendering using a series elastic interface with possible fluid power applications [5]. But SEA has not been widely adopted within the haptics community to date. SEA does involve compromises introduced by the elastic element. Perhaps most significantly, SEA devices are unable to passively render virtual environments stiffer than the series elastic element [11,13].

In this paper we undertake a side by side comparison of admittance display and what we shall call SEA display, with a focus on the range of impedances that may be displayed by either device across the frequency range. The advantage at high frequencies afforded by SEA display, where rendered impedance defaults to a lower inherent impedance, must be evaluated in parallel with the range of impedances that can be rendered at low frequencies. We first evaluate the fidelity with which either display can render freespace or a stiff virtual object. Our evaluation is presented in the frequency domain. We compare analytical results to experimental results produced with a platform that can be configured either for admittance display or SEA display. In the second part of the paper, we consider the upper limits on stiffness rendering imposed by an analysis of passivity. In our analysis of passivity we adopt an approach that accounts for an excess of passivity contributed by the biomechanics of the human user [2].

2 Model Description

2.1 Admittance Control Devices

Let us begin by describing admittance control in detail. A schematic model and block diagram model of an admittance-controlled device are shown in Fig. 1. Let M designate the effective mass of the rotor inertia reflected through the transmission to the stage which is grasped by the human user, and let B describe damping to ground. The user applies force F_u and a motor applies force F_m through a transmission with gear ratio n. A feedback controller $C(s)$ is used to close a loop so as to cause sensed force F_u to track the desired force F_{des}, which is specified as a response of the virtual environment Z_{VE} to $\dot{x}$. The inherent impedance of the haptic device is abbreviated as $Z_h = Ms + B$.

Since we care about what the user *feels*, it is appropriate to analyze the device in terms of driving point impedance $\mathcal{Z}$, the force-velocity relationship at the interface between the human and the haptic device. In terms of the variables used here, we therefore have $\mathcal{Z} \equiv F_u/\dot{X}$. Hence the closed-loop (powered - "P") driving point impedance in this architecture may be expressed as:

$$\mathcal{Z}^P_{ADM} = \frac{nC(s)Z_{VE} + Z_h}{nC(s) + 1}. \tag{1}$$

In this expression, we can see that the driving point impedance is shaped by tuning the feedback gain $C(s)$. As $C(s) \to \infty$, the driving point impedance converges to the virtual environment impedance: $\mathcal{Z}^P_{ADM} \to Z_{VE}$.

We also define the open loop driving point impedance (unpowered - "U"). This is found by substituting $C(s) = 0$ into Eq. (1), and is expressed as

$$\mathcal{Z}^U_{ADM} = Z_h. \tag{2}$$

As previously mentioned, the inherent open loop impedance Z_h is usually large (non-backdrivable) when admittance control is used. Inevitably, the rendered impedance will approach this mechanical impedance at high frequencies.

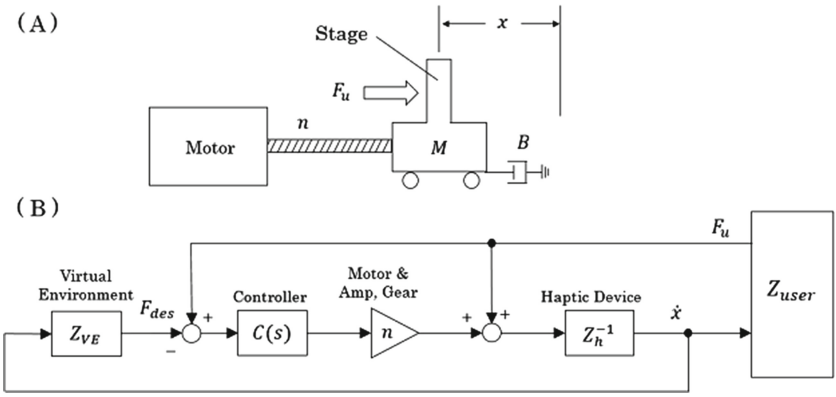

Fig. 1. Schematic model (A) and block diagram (B) of admittance control device

2.2 Series Elastic Actuator Device

We now introduce the control architecture of a haptic device that features a series elastic element. A schematic model and block diagram are presented in Fig. 2. As depicted in the diagram in part A, an elastic element (physical spring) is placed between the stage and end-effector. The force F_u applied by the user can be approximated if the relative displacement of the spring is measured and the spring constant is known: $F_u \simeq k(y-x)$. Thus a force sensor is not required.

The impedance of the end effector is $Z_e = ms$, and k and b are the stiffness and damping of the physical spring placed between stage and end-effector. The driving point impedance (powered - "P"), $\mathcal{Z} \equiv F_u/\dot{Y}$, can be found from this diagram to be:

$$\mathcal{Z}^P_{SEA}(s) = \frac{Z_e(Z_h + knC(s)/s + k') + k'(Z_h + nC(s)Z_{VE})}{Z_h + knC(s)/s + k'} \tag{3}$$

where $k' = k/s + b$. It should be noted that the rendered impedance does not converge to the virtual environment as feedback gain increases to infinity.

$$\mathcal{Z}^P_{SEA} \to Z_e + Z_{VE}\left(1 + \frac{b}{k}s\right), \quad (C(s) \to \infty). \tag{4}$$

This is because F_u has been approximated by neglecting the end-effector mass and damping. Since the end-effector is usually designed with a small mass compared to that of the stage ($m \ll M$) and the force is dominated by the spring k rather than damping b, this error between desired and rendered impedance is negligible.

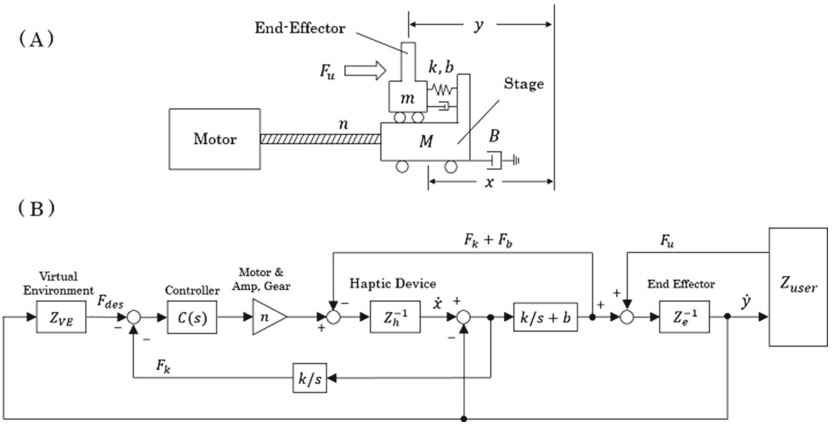

Fig. 2. Schematic model (A) and block diagram (B) of SEA haptic device.

By virtue of the physical spring, the SEA device has a low inherent (unpowered - "U") impedance:

$$\mathcal{Z}^U_{SEA} = Z_e + \frac{Z_h k'}{Z_h + k'}. \tag{5}$$

Visible here is the series coupling of two impedances, Z_e and $Z_h k'/(Z_h + k')$. The second impedance is essentially the parallel coupling of Z_h and k'. The elastic element masks Z_h, resulting in a smaller unpowered impedance than $\mathcal{Z}^U_{ADM}$.

2.3 Comparative Analysis

In the following, the virtual environment Z_{VE} is set to a constant stiffness, $Z_{VE}(s) = K_{VE}/s$, and the controller is set as a proportional gain, $C(s) = C_p$ for the sake of simplicity. One can examine the behaviors by analyzing $\mathcal{Z}$ in different extreme cases, as shown in Table 1.

Table 1. Comparative values of driving point impedance.

	$\omega \ll 1,\ K_{VE} \neq 0$	$\omega \ll 1,\ K_{VE} = 0$	$\omega \gg 1$
$\mathcal{Z}^P_{ADM}$	$\frac{nC_p}{nC_p+1}\frac{K_{VE}}{\omega}$	$\frac{B}{nC_p+1}$	$\frac{M}{1+nC_p}\omega$
$\mathcal{Z}^P_{SEA}$	$\frac{nC_p}{nC_p+1}\frac{K_{VE}}{\omega}$	$\frac{B}{nC_p+1}$	$m\omega$

At low frequencies, the apparent impedances for the admittance and SEA devices converge to the same values, while the impedances at high frequency diverge. The mass of the end-effector is very small compared to the stage ($m \ll M$), so generally the impedance in the SEA architecture is smaller than in the admittance architecture at high frequencies ($\omega \gg 1$).

These differences can also be viewed graphically. Figure 3 shows frequency plots of the driving point impedance magnitude for both the admittance display and SEA devices in both unpowered ($C(s) = 0$) and powered ($C(s) = C_p$)

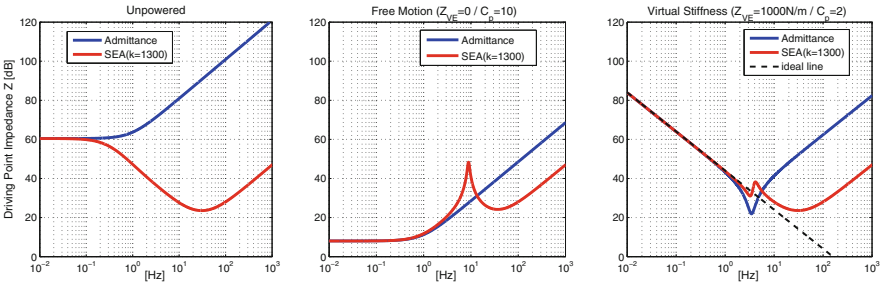

Fig. 3. Driving point impedance theoretical results. (Color figure online)

conditions. At low frequency both devices behave similarly for all three cases, but there is a large difference at high frequencies. Clearly for free motion (center figure), the lines should be as low as possible at all frequencies; except for a resonant spike, the SEA device achieves lower impedances as frequency increases. For rendering a virtual stiffness (right figure), both devices fail to achieve the desired stiffness as frequency increases, but the SEA device is able to render "spring-like" behavior up to a higher frequency.

3 Apparatus Description

We devised a single-axis system that could be configured either as an admittance display device or a Series Elastic Actuator. Figure 4 shows a CAD rendering of the apparatus and Fig. 5 shows a photograph of the device. As is typical in admittance- and SEA-display devices, a high gear ratio ball screw (5 mm pitch, SFU series 1605) is attached to the motor (Maxon RE65 #353295). While this allows large forces to be sourced, it makes the apparent mass of the motor and ballscrew shaft n^2 times higher and friction on the screw n times higher. These values reflected through the gear ratio, along with other relevant parameters estimated through system identification, are provided in Table 2. These large friction and inertia values render the carriage totally non-backdrivable — when the motor is unpowered, a human pushing on the stage cannot move the motor at all. An encoder (US Digital E2-1024) attached to the back shaft of the motor measures the shaft angle. A linear encoder (US Digital EM1-0-500-N) measures the relative displacement $(x-y)$ between the stage and end-effector, which yields the compression of the physical spring. For the admittance display setup, the proximal side of a beam load cell (Transducer Techniques LSP-10) is attached to the stage. The distal side of this load cell is grasped by the user. Control and data acquisition are performed with Visual Studio/C++, using a Sensoray Model 626 card.

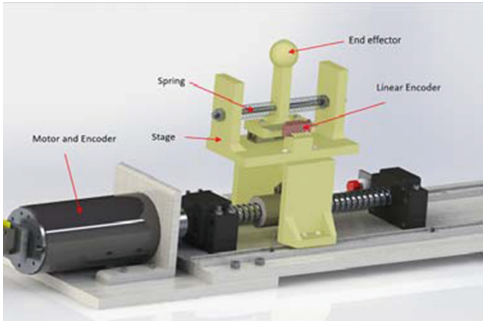

Fig. 4. SolidWorks design rendering

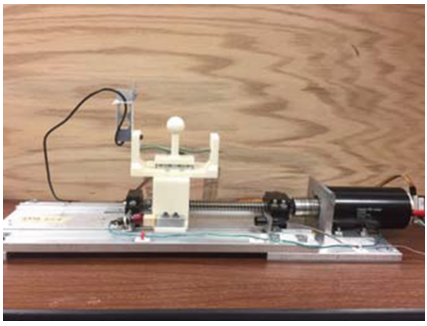

Fig. 5. Apparatus for haptic rendering

Table 2. Physical device parameter values from system ID.

	Symbol	Value	Units
Stage and motor inertia	M	176	[kg]
Stage damping	B	1051	[kg/s]
End-effector mass	m	0.035	[kg]
End-effector damping	b	15.05	[kg/s]
Physical spring stiffness	k	1300	[N/m]
Gear ratio	n	41.8	[-]

4 Experimental Results

Using the two configurations of the apparatus described in the previous section (SEA and admittance), we ran a number of experimental tests to validate the analytical findings. For each configuration, data was collected in three conditions, matching those simulated in the analytical work: unpowered, powered rendering free space, and powered rendering a stiffness. In each case, manual excitation of the device was performed. The results of these tests are shown in Fig. 6 in the frequency domain, along with the analytical curves previously shown in Fig. 3.

The left pane of Fig. 6 shows the open-loop impedance $\mathcal{Z}^U$ ($C_p = 0$). The SEA device response matched the model fairly well, but the admittance device had a significant offset from the modeled impedance. In reality, the stage is not backdrivable at all, largely due to unmodeled stiction.

The middle pane of Fig. 6 shows the driving point impedance for both devices rendering free motion. At low frequencies, both devices performed similarly, comparable with the analytical prediction. As the frequency increased, the two device configurations' responses diverged. At high frequencies, the SEA device rendered lower admittances when trying to achieve free space; this effect is visible at the high end of human motion generation, up to about 20 Hz [12].

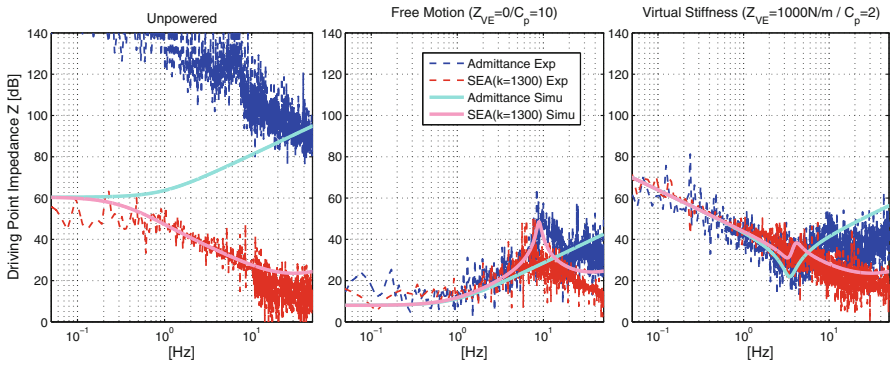

Fig. 6. Driving point impedance experimental results. (Color figure online)

The same situation is visible in the right pane of Fig. 6 which shows the two devices rendering a virtual spring ($K_{VE} = 1000N/m$). Again, the devices are comparable at low frequencies. As frequency increases, both devices diverge from the ideal stiffness, but the SEA device exhibits higher fidelity (the desired and achieved responses are more similar).

As is evident from both analytical and experimental results, SEA holds an advantage over the admittance display device in terms of backdrivability and high frequency performance. While this analysis has allowed us to compare free space rendering and fidelity, we have not yet examined the upper limits of stiffness rendering for each device. These limits follow from a loss of stability of the coupled human-device system; thus, we take up the topic of stability.

5 Passivity Limits on Rendered Springs

One method for guaranteeing the coupled stability of the system comprising human user and haptic interface is to assume the human user is passive and require the haptic device to adhere to strict passivity [4]. Justification for the assumption of human passivity is made with reference to the literature [6]. Necessary and sufficient conditions for passivity of a 1-port system are

$$1.\ \mathcal{Z}(s) \text{ has no poles in the right half plane, and} \tag{6}$$

$$2.\ Re(\mathcal{Z}(j\omega)) > 0, \tag{7}$$

where $\mathcal{Z}(s)$ is the driving point impedance [3].

Under ideal conditions (linearity holds, without sampling or saturation effects), the admittance control device is passive. SEA on the other hand is not passive, even under ideal conditions. Consider first the passivity of the transfer function $\dot{Y}/F_u$ for SEA Display. If $b = 0$ is assumed for simplicity, the condition that places the poles of this transfer function in the left-half plane is found by application of the Routh-Hurwitz criterion:

$$K_{VE} < \frac{1 + nC_p}{nC_p} k. \tag{8}$$

In general, nC_p has a large value by hardware and control design. Therefore, the virtual stiffness must be smaller than the physical spring stiffness to achieve passivity. This was observed by Vallery et. al. [13], who also applied passivity analysis to series elastic actuators. This challenge was recently discussed in [11], where coupled stability analysis was undertaken for sampled-data SEA devices, resulting in a calculation of the minimum necessary coupled mass to achieve stability above the physical spring stiffness.

The sampling and zero order hold (ZOH) processes, inherent in any sampled-data controller, may have an effect on stability, so we take them into account for our passivity analysis. We rewrite the motor command as a sampled and held signal and approximate the Laplace representation of a ZOH, $(1 - e^{-sT})/(sT)$ (where T is the sampling time step), with a first order Padé approximation as

$1/(\tau s + 1)$ where $\tau = 1/2T$. From this form it is clear that sampling introduces a time delay of τ. Thus, the maximum stiffness K_{VE} that can be rendered by an admittance device at any given frequency is a function of the sampling rate T and the feedback gain C_p. For an SEA device, the upper stability limit on K_{VE} depends on C_p and T, as well as the physical spring stiffness k.

It has been shown that in the presence of any delay/sampling, an admittance display device without a virtual coupling to limit the virtual environment is no longer unconditionally passive [1]. One way to address this challenge is to introduce a model of the human that includes a minimum and maximum impedance, reducing the conservativeness of the analysis. Limits on the maximum impedance Z_{max} and minimum impedance Z_{min} of the human were handled in [2] by placing two constant impedances $Z_1 = Z_{min}$ and $Z_2 = Z_{max} - Z_{min}$ respectively in series and in parallel with a variable human impedance Z_p. If Z_p is zero, the presented impedance is $Z_1 = Z_{min}$ and if Z_p is infinity, the impedance becomes $Z_2 - Z_1 = Z_{max}$. To reduce the conservativeness of the passivity analysis, the driving point impedance can be re-written to absorb these constant limiting portions of this human arm model, yielding:

$$\mathcal{Z}' = \left(\frac{1}{Z_2} + \frac{1}{Z_1 + \mathcal{Z}}\right)^{-1} = \frac{Z_2(Z_1 + \mathcal{Z})}{Z_1 + Z_2 + \mathcal{Z}}. \tag{9}$$

In this paper we adopt the approach introduced in [1] and apply it to both Admittance Display using Eq. 1 for $\mathcal{Z}$, and to SEA Display using Eq. 3 for $\mathcal{Z}$.

We do not limit the minimum impedance — we use $Z_{min} = 0$ so as to cover cases with no contact. For maximum impedance, we borrow from [2] again and set $Z_{max}(s) = 300 + 1000/s$. This was in turn based on previous research [7], which shows that human arm impedance can be approximated as a damper and spring. These values pertained to the whole arm, whereas our device is only grasped with the fingers, so we acknowledge that our results may not be sufficiently conservative.

Our objective is to render an arbitrary virtual environment to the user, but here we only assess the range of virtual stiffnesses that can be rendered passively by the Admittance and SEA Display devices. We assess passivity by checking the expression for $\mathcal{Z}'$ against the conditions in Eqs. 6 and 7 for a range of values for the following parameters: control gain C_p, sampling time T, stiffness k of the series elastic element for SEA Display, and virtual environment stiffness K_{VE}.

The sampling rate imposes an upper limit on what virtual environment stiffness K_{VE} may be rendered passively for both the SEA and admittance devices, as shown in Fig. 7A. Values for the control gain $C_p = 2$ and compliant element stiffness $k = 1300$ N/m were chosen to match the values used in the experiments described above. The limiting effects of stiffness k on virtual stiffness rendering for SEA can be seen in Fig. 7B. When a systematic search of T and C_p (and k for SEA) is performed, an upper limit on the virtual stiffness that can be passively rendered may be found. For our device, the sampling time was variable, but averaged about 1 ms, as indicated.

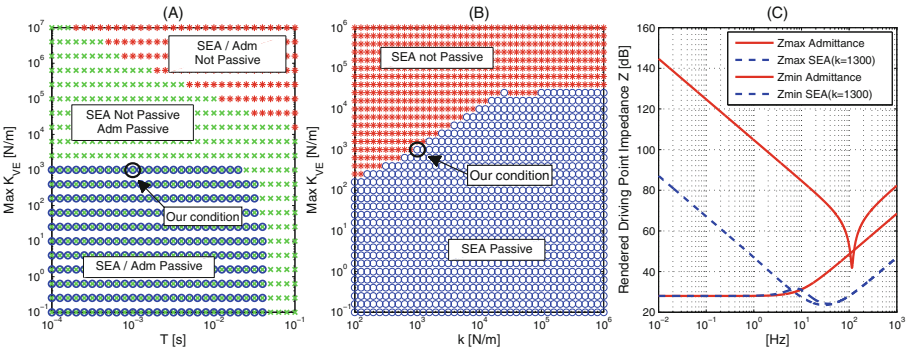

Fig. 7. (A) Effect of sampling rate on passivity for SEA ($k = 1300$) and admittance devices, both at $C_p = 2$. Approximate experimental condition indicated. Blue circles indicate passivity-satisfying conditions for SEA, green x's indicate passivity for admittance, and red stars indicate non-passive conditions. (B) Effect of SEA physical stiffness k on passivity. Approximate experimental condition indicated. (C) Limits of passively renderable K_{VE}/s for SEA and admittance devices. (Color figure online)

On the other hand, the minimum virtual stiffness does not come from the stability analysis, but is achieved when $Z_{VE} = 0$. To realize an accurate virtual environment, high feedback gain is needed. Thus in our allowed feedback gain range, the minimum impedance is rendered by setting $Z_{VE} = 0$ and $C_p = 10$.

Figure 7C shows the limits on the range of virtual stiffnesses which can be rendered by our device while maintaining passivity. At low frequencies, the advantage of the admittance device is clear: it can render higher stiffness passively. However, as frequency increases, the rendering of pure stiffness breaks down, and both devices revert to an impedance that feels like a mass — a small mass with the SEA device, and a large mass with the admittance device.

6 Conclusion

In this work, we made a direct comparison between the limitations, performance, and stability of admittance and series elastic haptic devices. By employing a reconfigurable experimental platform, we were able to make this comparison not only analytically, but also experimentally. For free-space rendering, SEA and admittance devices perform comparably at low frequencies, but at the high end of the human motor generation frequency range the user feels only the mass of the end effector with SEA, while the admittance device reflects the rotor inertia through the gear ratio and results in higher impedances. The "free-er" free space of the SEA device, however, comes at the expense of stiff virtual walls, since passivity analysis shows that SEA cannot render walls as stiff as admittance can. However, since applications exist for which impedance-controlled devices are currently considered stiff enough, this trade-off may be desirable in some applications.

Naturally, the picture concerning all the trade-offs in the design of an impedance, admittance, or SEA display device is still incomplete. Additional considerations would include force and speed saturation by the electromagnetic actuators, and perhaps effects of stiction. Admittance-controlled devices and impedance-controlled devices are generally designed with their end-use in mind, and as such they typically use drastically different hardware designs. However, valuable insight might be gained from experiments with an "intermediate" hardware design (lightly geared, but still possible to backdrive, trading off force and backdrivability) that could be configured for use with admittance control or impedance control, or fitted with springs to realize a series elastic actuator.

Acknowledgments. This research was supported by NIH grant R01-EB019834 and NSF grant DGE 1256260.

References

1. Adams, R.J., Hannaford, B.: Stable haptic interaction with virtual environments. IEEE Trans. Robot. Autom. **15**(3), 465–474 (1999)
2. Adams, R.J., Hannaford, B.: Control law design for haptic interfaces to virtual reality. IEEE Trans. Control Syst. Technol. **10**, 3–13 (2002)
3. Colgate, E., Hogan, N.: An analysis of contact instability in terms of passive physical equivalents. In: Proceedings of IEEE International Conference on Robotics and Automation, pp. 404–409 vol.1, May 1989
4. Colgate, J.E., Hogan, N.: Robust control of dynamically interacting systems. Int. J. Control **48**(1), 65–88 (1988)
5. Gillespie, R.B., Kim, D., Suchosk, J.M., Bo, Y., Brown, J.D.: Series elastic for free free-space motion for free. In: IEEE Haptic Symposium, pp. 609–615 (2014)
6. Hogan, N.: Controlling impedance at the man/machine interface. In: International Conference on Robotics and Automation (ICRA), pp. 1626–1631 (1989)
7. Mussa-Ivaldi, F.A., Hogan, N., Bizzi, E.: Neural, mechanical, and geometric factors subserving arm posture in humans. Neuroscience **5**, 2732–2743 (1985)
8. Pratt, G.A., Williamson, M.M.: Series elastic actuators. In: IEEE/RSJ International Conference on Intelligent Robots and Systems. Human Robot Interaction and Cooperative Robots, vol. 1, pp. 399–406 (1995)
9. Pratt, J., Krupp, B., Morse, C.: Series elastic actuators for high fidelity force control. Ind. Robot Int. J. **29**(3), 234–241 (2002)
10. Robinson, D.W.: Design and analysis of series elasticity in closed-loop actuator force control. Ph.D. thesis (2000)
11. Sergi, F., O'Malley, M.K.: On the stability and accuracy of high stiffness rendering in non-backdrivable actuators through series elasticity. Mechtronics **26**, 54–75 (2015)
12. Tan, H.Z., et al.: Human factors for the design of force-reflecting haptic interfaces. Dyn. Syst. Control **55**(1), 353–359 (1994)
13. Vallery, H., Veneman, J., van Asseldonk, E., Ekkelenkamp, R., Buss, M., van Der Kooij, H.: Compliant actuation of rehabilitation robots. IEEE Robot. Autom. Mag. **15**(3), 60–69 (2008)
14. Vanderborght, B., Albu-Schaeffer, A., et al.: Variable impedance actuators: a review. Robot. Auton. Syst. **61**(12), 1601–1614 (2013)